Taut cables with hanging masses: A metamaterial-like dynamic behavior

Marco Moscatelli, Claudia Comi, Jean-Jacques Marigo

European Journal of Mechanics / A Solids 106 (2024) 105330

Contents lists available at ScienceDirect

European Journal of Mechanics / A Solids

journal homepage: www.elsevier.com/locate/ejmsol

Full Length Article

Taut cables with hanging masses: A metamaterial-like dynamic behavior

Marco Moscatelli [a,*], Claudia Comi [a], Jean-Jacques Marigo [b]

[a] Department of Civil and Environmental Engineering, Politecnico di Milano, Piazza Leonardo da Vinci 32, 20133 Milan, Italy
[b] Institute Jean Le Rond d'Alembert, Sorbonne Université, 4 place Jussieu, Paris 75005, France

ARTICLE INFO

Keywords:
Metamaterial
Wave localization
Cable dynamics
Band gaps

ABSTRACT

We inspect the dynamic behavior of suspended cables presenting a periodic array of scatter elements, consisting of a discrete set of masses that are hanging by means of elastic or rigid connections. By introducing some approximations, we show that the problem in the continuous domain can be brought back to an equivalent discrete problem, whose solutions depend on the variation of an effective mass. We find that the essential spectrum of the problem presents band gaps. By considering boundary conditions, eigenmodes can only be found at frequencies belonging to pass bands for the propagation problem of the unbounded system. This is no more true when a defect of periodicity is inserted, leading to the formation of localized modes. We provide a quantitative validation of these theoretical results by means of comparison with experimental tests.

1. Introduction

Cables are used as structural solutions in many applications, such as for the mooring and towing of marine vehicles or platforms, for overhead lines, for roofing systems, for cable-stayed and suspension bridges, or as guy-wires to add stability to a free-standing structure. Structural cables can present a family of objects, such as weights, instruments or buoyancy elements, either directly attached or hanging along them, very often in a periodic fashion. In many cases they can be considered as punctual masses, obtaining the structural scheme represented in Fig. 1. Systems of this type can model for instance overhead lines presenting Stockbridge dampers or marker balls, and cableways. Likewise, the main cable in suspension bridges supports the deck by means of a set of hangers distributed along it; a preliminary assessment may consider the deck to be very flexible (see e.g. the fundamental work of Irvine (1981)), reducing its effect on the cable dynamics to that of suspended equivalent masses.

Beyond the practical interest, the dynamics of cables has attracted large attentions in the scientific community due to the variety of their behavior (Rega, 2004a,b). As engineering cables are usually lengthy and flexible, their steady-state vibrations can involve large displacements and are often dominated by geometric non-linearities. This can lead to the activation of different phenomena, such as hardening or softening at a primary resonance response, secondary and internal resonances, and parametrically excited responses, to name but a few (Nayfeh and Mook, 1995; Nayfeh and Frank Pai, 2008).

The dynamics of cables can be strongly modified by the presence of attached resonating or scattering elements. In this work, we analyze the wave propagation problem and we show that, already in the linear regime of small oscillations, cables with a periodic arrangement of masses can be subjected to extremely interesting phenomena, crucial to understand their dynamics. As pointed out in Demeio and Lenci (2022), where taut cables with continuously attached bilinear strings were studied, there exist surprisingly few results on the above-mentioned problem. Furthermore, the same equation treated here governs the axial and torsional dynamic response in beams, with other important practical applications.

The propagation of waves in periodic domains is a central topic when dealing with the so-called metamaterials (or metastructures), i.e. systems with a microstructure designed in a way to obtain peculiar properties. In dynamics, waves can interact with the microstructure generating a banded spectrum and enabling for the control and manipulation of their propagation. This phenomenon was first noticed and analyzed in the context of electromagnetism (Joannopoulos et al., 2008) and then identified also in the context of elasticity and acoustics (Laude, 2015). Nowadays, applications based on this dynamic behavior have been extensively studied, for instance to obtain efficient wave shields (Miniaci et al., 2016; Palermo et al., 2016), compact absorbers (Maurel et al., 2018), cloaking devices (Schurig et al., 2006; Milton et al., 2006; Torrent and Sánchez-Dehesa, 2008) and superlenses (Pendry, 2000; Yang et al., 2015).

In the present work we study the dynamic behavior of taut cables with periodically distributed point-wise hanging masses by interpreting these systems as particular metastructures. Specifically, we show that cables with hanging masses can be characterized by the presence of

* Corresponding author.
E-mail address: marco.moscatelli@polimi.it (M. Moscatelli).

https://doi.org/10.1016/j.euromechsol.2024.105330
Received 13 February 2024; Received in revised form 15 April 2024; Accepted 23 April 2024
Available online 25 April 2024

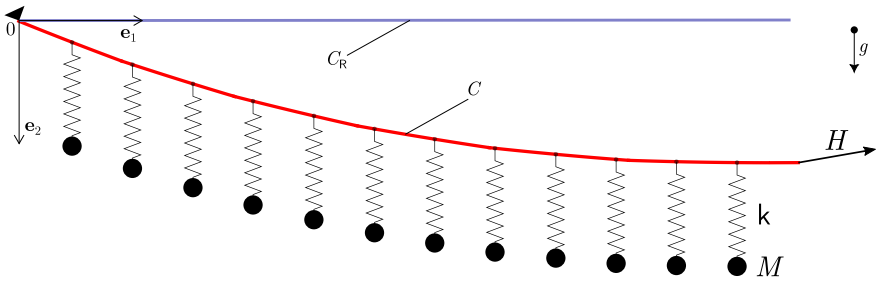

Fig. 1. A cable with reference configuration $\mathcal{C}_R$ and equilibrium configuration $\mathcal{C}$ is suspended between a support on the left-hand side and an applied force on the right-hand side, with a discrete and periodic set of hanging masses. The cable is subjected to the gravity field $g\boldsymbol{e}_2$.

band gaps in their dynamic behavior. This information results to be important for the prediction of their modal response. In particular, for a real system with finite spatial dimensions (i.e. taking into account boundary conditions), the eigenmodes can only appear at frequencies outside the predicted band gaps. More in general, the findings of this work can be of great interest for the metamaterial community, for instance to design tensegrity structures, where the system can be tuned to vary its dynamic response (He et al., 2022).

In real-life cable systems, exact periodicity is never met due to the presence of local defects. These can be generated, for instance, by a non-perfect periodic repetition or a deficient attachment of the hanging elements.

It is well known that the dynamics of a periodic domain is strongly altered by the presence of defects. Specifically, the system can support a localized behavior that decays away from the defect. This phenomenon was first noticed for cases with distributed imperfections at a microscopic scale in solid state physics (Anderson, 1958), and then studied at a macroscopic scale for classical waves in lattice models (Figotin and Klein, 1994) and continuous domains (Figotin and Klein, 1996). It was later shown that, if instead of distributing the imperfections all over the domain of the problem, one considers a single (or a few) compact defect(s), localization can still be activated, provided that the system sustains the formation of band gaps (Figotin and Klein, 1997). Metamaterials and metastructures of the type described before can thus experience the localization phenomenon. This peculiar behavior was both numerically and experimentally studied (Sigalas, 1997, 1998; Wilcox et al., 2005; Fliss and Joly, 2012).

The phenomenon is of particular interest as it offers attractive solutions for the design of highly efficient waveguides: by combining several defects, localization has been effectively exploited to build metamaterials able to control and guide the propagation of waves (Khelif et al., 2003; Santosa and Ammari, 2004; Laude, 2021; Krushynska et al., 2021; Ammari et al., 2022). For cables of civil engineering applications, a localized dynamic motion can be unfavorable for safety requirements, but, if controlled, can also be employed to focus the energy of ambient oscillations in specific regions for energy harvesting (Rosafalco et al., 2023).

In this work, we complement the aforementioned references by proving both theoretically and experimentally the existence of localized responses created by a geometrical perturbation of a particular periodic medium. More specifically, we demonstrate that defective cable structures can be affected by localized modes in their spectrum and that this phenomenon can be easily explained by exploiting our novel approach to the interpretation of their dynamic behavior. This new perspective to the problem can in principle be used to facilitate the modeling and assessment of periodic cable systems, found in real-life applications.

The rest of the paper is organized as follows. In Section 2, we analyze the dynamics of cables with hanging masses and show that their behavior can be governed by an effective equation valid for periodic lattice media. In Section 3, we first derive the pass and stop bands of the continuous spectrum and we then consider the problem in a bounded domain to study the relation between the associated eigenvalues and the band gaps computed for the unbounded domain. A localization phenomenon is obtained by inserting a defect of periodicity. All the theoretical results are validated experimentally in Section 4. Some concluding remarks and future perspectives are finally given in Section 5.

Notation: spatial derivatives are denoted as $(\bullet)'(x,t) := \partial\bullet/\partial x$, while time derivative as $\dot{(\bullet)}(x,t) := \partial\bullet/\partial t$; an overline $\overline{(\bullet)}$ is used for the closure of a set; the imaginary unit of a complex number or field is denoted with the sans serif letter j.

2. The dynamics of cables with hanging masses

Let us consider a heavy inextensible cable in tension between two supports at distance ℓ and placed at the same height, as shown in Fig. 2, with the particles (black circles) representing a mass M hanging on the cable by means of a mass-less elastic spring of stiffness k. The left end is fixed, while the right end is free to move horizontally and it is subjected to an external horizontal force $H_{\text{eq}}(1 + h(t))$. We refer to Moscatelli (2022) for a detailed revision on the validity of this model.

In this section, we shall derive an effective wave equation governing the dynamics of the system under consideration.

2.1. Preliminaries

The natural configuration of the cable is the curve $S \to \boldsymbol{x}_R(S)$, with $\boldsymbol{x}_R \in \mathbb{R}^2$, being parametrized by its curvilinear abscissa $S \in (0, \ell_R)$ (cf. Fig. 2). In what follows, we use the subscript "R" to indicate a quantity in the reference configuration, that is taken to be horizontal.

Let us make here the following assumptions:

- The cable is inextensible and perfectly flexible (by definition), with linear mass density ρ_R and area A_R in the reference configuration;
- The Poisson's effect is neglected, meaning that the area A at any time t will remain equal to A_R;
- The masses are equally spaced, the distance between two masses being $d = \ell_R/(n+1)$ (accordingly the ith mass is attached to the cable at the point $S_i = id$). The set containing the curvilinear abscissas of the points where a punctual mass can be found is called $\mathcal{P} \subset \mathcal{C}_R$, with $\mathcal{C}_R = (-\infty, +\infty)$;
- Both the cable and the masses are placed in the gravity field $g\boldsymbol{e}_2$;
- At a point S_i the masses attached along the cable are assumed to transmit only a concentrated vertical force F_i to the cable, and thus no pendulum motion is possible.
- The applied force is much larger than the total weight of cable and attached masses
- The vibrations of the cable around the equilibrium configuration are small.

We denote by $\boldsymbol{x}_{\text{eq}}(S)$ the position of the material point S in the static equilibrium configuration $\mathcal{C}_{\text{eq}}$ and $\boldsymbol{x}(S,t)$ that in the configuration $\mathcal{C}$ of the cable in motion at time $t \in [0, +\infty)$. We call $\boldsymbol{u}(S,t)$ the difference between the configurations $\boldsymbol{x}(S,t)$ and $\boldsymbol{x}_{\text{eq}}(S)$, such that

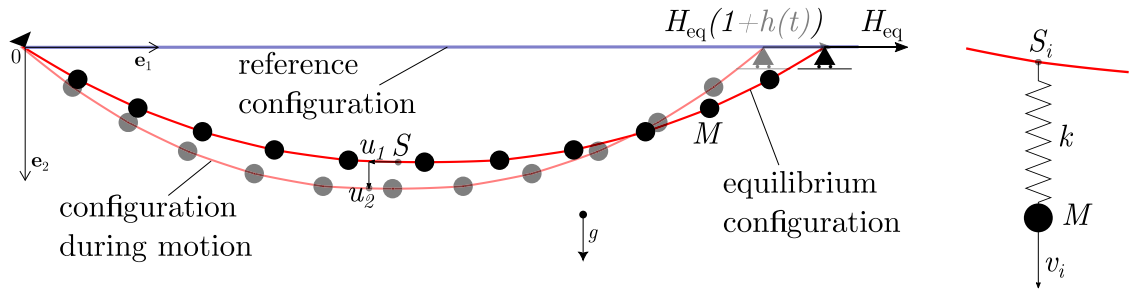

Fig. 2. The in-plane motion problem associated to a cable with a discrete and periodic set hanging masses.

$\boldsymbol{u}(S,t) = \boldsymbol{x}(S,t) - \boldsymbol{x}_{\rm eq}(S)$. We consider $\boldsymbol{x}(S,t)$ and its derivative in time $\dot{\boldsymbol{x}}(S,t)$ to be continuous on $\{C_{\rm R} \times [0,+\infty)\}$, with null values for $(S,t) = \{\overline{C}_{\rm R} \times 0\}$. We will use a subscript "eq" to refer to a quantity in the configuration $C_{\rm eq}$.

Since the flexural moment is null, and thus already fixed, we cannot control the orientation of the cable (i.e. the angle between its tangent and direction $\boldsymbol{e}_1$). As a consequence, its motion is not necessarily "regular" and its space of definition must be enlarged. In particular, the configuration $S \to \boldsymbol{x}(S)$ will always be continuous, but only piecewise differentiable.

The motion of the cable is thus governed by the following equation:

$$(N\boldsymbol{t})'(S,t) + \rho_{\rm R} g \boldsymbol{e}_2 - \rho_{\rm R} \ddot{\boldsymbol{x}}(S,t) = \boldsymbol{0}, \quad \forall S \in C_{\rm R} \backslash \mathcal{P}, \ \forall t, \tag{1}$$

where $N(S,t)$ is the amplitude of the axial force and $\boldsymbol{t}$ is the unit vector tangent to the curve, such that:

$$\boldsymbol{t}(S,t) = \boldsymbol{x}'(S,t), \quad \|\boldsymbol{x}'(S,t)\| = 1. \tag{2}$$

At the points $S_i \in \mathcal{P}$, the vertical displacement v_i of the end point of the spring where the ith mass is attached can be determined from the following jump condition

$$[\![(N\boldsymbol{t})]\!](S_i,t) + F_i \boldsymbol{e}_2 = \boldsymbol{0} \tag{3}$$

where the punctual force $F_i(t)$, transmitted by the spring, is obtained by enforcing the linear momentum balance as

$$F_i(t) := k(v_i(t) - x_2(S_i,t)) = M\left(g - \ddot{v}_i(t)\right) \tag{4}$$

Interestingly, the structural model just described can be used to analyze the case when the masses are directly attached to the cable: one can consider the stiffness $k \to +\infty$ and thus obtain that $v_i(t) = x_2(S_i,t)$ for the force F_i to be bounded.

The motion problem of the system is finally completed by imposing the conditions at the boundaries, such that:

$$\boldsymbol{x}(0,t) = \boldsymbol{0}, \quad x_2(\ell_{\rm R},t) = 0 \quad \text{and} \quad (Nt_1)(\ell_{\rm R},t) = H_{\rm eq}(1+h(t)). \tag{5}$$

2.2. The effective mass

Let us first consider the static equilibrium configuration of the cable. When, as here assumed, the intensity of the horizontal force $H_{\rm eq}$ is much larger than the total weight of the cable and attached masses, the static equilibrium configuration tends to become horizontal ($x_{2(\rm eq)}(S) = 0$), and the tension in the cable tends to be uniform and equal to the applied force ($N_{\rm eq}(S) = H_{\rm eq}$). Note that the assumption of a horizontal equilibrium configuration is crucial for the following developments. Its pertinence to real problems should be carefully checked for each specific case.

We here consider small harmonic vibrations of the system around its horizontal equilibrium configuration. For this, the time variation $h(t)$ of the force applied at the right end of the cable can be written as

$$h(t) = H \exp\{\mathrm{j}\omega t\}, \tag{6}$$

with the dimensionless amplitude H assumed to be small. We thus seek formal solutions of the initial boundary value problem specified hereabove by considering that the motion $\boldsymbol{u}(S)$ of the cable and v_i of the generic ith mass remain close to their stable equilibrium configurations, such that

$$\begin{cases} N(S,t) = N_{\rm eq}(S) + H_{\rm eq}\hat{N}(S)\exp\{\mathrm{j}\omega t\}, \\ \boldsymbol{x}(S,t) = \boldsymbol{x}_{\rm eq}(S) + \ell_{\rm R}\hat{\boldsymbol{u}}(S)\exp\{\mathrm{j}\omega t\}, \\ v_i(t) = v_{i(\rm eq)} + \ell_{\rm R}\hat{v}_i(S)\exp\{\mathrm{j}\omega t\}, \end{cases} \tag{7}$$

where $\hat{N}$, $\hat{\boldsymbol{u}}$ and $\hat{v}_i$ are small dimensionless quantities, of the same order of magnitude of the dimensionless prescribed force amplitude H.

By introducing the dimensionless coordinate $\hat{S}$ and the dimensionless fields $\hat{N}_{\rm eq}$, $\hat{\boldsymbol{x}}_{\rm eq}$ as

$$\hat{S} = S/\ell_{\rm R}, \quad \hat{N}_{\rm eq} = N_{\rm eq}/H_{\rm eq}, \quad \hat{\boldsymbol{x}}_{\rm eq} = \boldsymbol{x}_{\rm eq}/\ell_{\rm R}, \tag{8}$$

the static equilibrium configuration is characterized by (see Moscatelli, 2022):

$$\hat{N}_{\rm eq}(\hat{S}) = 1, \quad \hat{x}_{1(\rm eq)}(\hat{S}) = \hat{S}, \quad \hat{x}_{2(\rm eq)}(\hat{S}) = 0, \quad \forall \hat{S}. \tag{9}$$

Using the inextensibility condition given by the second of relations (2) and the boundary condition at $\hat{S} = 0$ from (5), one has:

$$\hat{u}_1(\hat{S}) = 0, \quad \forall \hat{S}. \tag{10}$$

The axial force $\hat{N}$ along the cable can then be derived from Eqs. (1) and (3) written for the horizontal direction, and the boundary condition (5) at $\hat{S} = 1$, obtaining:

$$\hat{N} = \hat{N}_{\rm eq}(1)\, H. \tag{11}$$

By using the above relation (11), Eq. (1) along the vertical direction can be rewritten as

$$\hat{u}_2''(\hat{S}) + (n+1)^2\Omega^2\hat{u}_2(\hat{S}) = 0, \quad \forall \hat{S} \in \left(\frac{i-1}{n+1}, \frac{i}{n+1}\right), \ 1 \le i \le n+1, \tag{12}$$

where Ω is a dimensionless frequency defined as:

$$\Omega = \omega\sqrt{\frac{\rho_{\rm R} d^2}{H_{\rm eq}}}. \tag{13}$$

Integrating relation (12) in the ith interval leads to:

$$\hat{u}_2(\hat{S}) = \frac{\hat{u}_{2(i)}\sin\Omega((n+1)\hat{S} - i + 1) + \hat{u}_{2(i-1)}\sin\Omega((n+1)\hat{S} - i)}{\sin\Omega}, \quad \forall \hat{S} \in \left(\frac{i-1}{n+1}, \frac{i}{n+1}\right) \tag{14}$$

where

$$\hat{u}_{2(i)} = \hat{u}_2(\hat{S}_i), \quad 1 \le i \le n. \tag{15}$$

From relation (4), the motion of the hanging masses can be determined, such that:

$$\hat{v}_i = \hat{u}_2(\hat{S}_i) \qquad \text{masses directly on the cable,} \tag{16}$$

$$\hat{v}_i = \frac{\hat{\mathsf{k}}}{\hat{\mathsf{k}} - \Theta\Omega^2}\hat{u}_{2(i)} \qquad \text{masses hanging with springs,} \tag{17}$$

for $1 \leq i \leq n$, with $\hat{\mathsf{k}}$ and Θ being respectively the dimensionless parameter associated with the stiffness of the springs, and the ratio between the mass of one hanging mass and the mass of the cable between two successive masses:

$$\hat{\mathsf{k}} = \frac{kd}{H_{\text{eq}}}, \quad \Theta = \frac{M}{\rho_{\text{R}} d}. \tag{18}$$

Relation (3) in the vertical direction finally gives the discrete linear system of effective equations, governing the displacements $\hat{u}_{2(i)}$ of the cable points above the hanging masses. Specifically, inserting relations (14) and (16) or (17) into Eq. (3) leads to the following equation

$$\Delta_i \hat{u}_2 + \mu(\Omega)\hat{u}_{2(i)} = 0 \quad \text{for} \quad i \in \mathbb{Z}, \tag{19}$$

where $\Delta_i(\bullet)$ denotes the discrete Laplacian operator

$$\Delta_i(\bullet) := (\bullet)_{i+1} + (\bullet)_{i-1} - 2(\bullet)_i \quad \text{for} \quad i \in \mathbb{Z} \tag{20}$$

and where $\mu(\Omega)$, defined as

$$\mu(\Omega) := \begin{cases} 2(1-\cos\Omega) + \Theta\Omega\sin\Omega & \text{masses directly on the cable} \\ 2(1-\cos\Omega) + \dfrac{\hat{\mathsf{k}}\Theta\Omega\sin\Omega}{\hat{\mathsf{k}} - \Theta\Omega^2} & \text{masses hanging with springs} \end{cases}, \tag{21}$$

that can be interpreted as a (dimensionless) equivalent mass that is a function of a normalized frequency Ω. Therefore, Eq. (19) gives an effective description of the system. It is noteworthy that Eq. (19), with proper definition of the equivalent mass $\mu(\Omega)$, also governs the dynamic behavior of 1D periodic systems of discrete mass and spring elements, see Moscatelli et al. (2021). This analogy allows to interpret the considered cable as a metamaterial.

Finally, The remaining boundary conditions (5) at $\hat{S} = 0$ and at $\hat{S} = 1$ fix the value of the vertical displacement at the two ends:

$$\hat{u}_{2(0)} = 0, \tag{22}$$

$$\hat{u}_{2(n+1)} = 2\hat{u}_{2(n)}\cos\Omega. \tag{23}$$

3. Metamaterials-like behavior

3.1. Band gaps

Solutions to Eq. (19) for $i \in \mathbb{Z}$ can be found in the form $\hat{u}_{2(i)} = r^i$. Inserting it into Eq. (19), one obtains the second order characteristic equation

$$r^2 - 2\left(1 - \frac{\mu}{2}\right) r + 1 = 0. \tag{24}$$

Solutions to Eq. (24) depends on whether $|(1-\mu/2)| < 1$ or $|(1-\mu/2)| > 1$, namely (see Moscatelli et al., 2021 for details):

- For $0 < \mu(\Omega) < 4$, the general solution reads:

$$\hat{u}_{2(i)} = a_1 \exp\left\{-\mathrm{j}\mathsf{K}^* i\right\} + a_2 \exp\left\{\mathrm{j}\mathsf{K}^* i\right\} \quad \text{with} \quad \mathsf{K}^* \in [0, \pi] \tag{25}$$

  and corresponds to a superposition of a right- and left-propagating waves;
- For $\mu(\Omega) < 0$ and $\mu(\Omega) > 4$, the general solutions read respectively:

$$\begin{aligned} &\hat{u}_{2(i)} = a_1 \exp\left\{-\mathsf{K}^* i\right\} + a_2 \exp\left\{\mathsf{K}^* i\right\}, \\ &\hat{u}_{2(i)} = a_1(-1)^i \exp\left\{-\mathsf{K}^* i\right\} + a_2(-1)^i \exp\left\{\mathsf{K}^* i\right\} \end{aligned} \tag{26}$$

  and correspond to a superposition of attenuated waves.

When $\mu = 0$ and $\mu = 4$, i.e. when $|(1-\mu/2)| = 1$, the solutions to the characteristic equation (24) are double roots and one can look for solutions of Eq. (19) in the form $\hat{u}_{2(i)} = r^i$ and $\hat{u}_{2(i)} = ir^i$. The general solutions then become:

$$\hat{u}_{2(i)} = \begin{cases} a_1 + ia_2 & \text{when } \mu = 0 \\ (-1)^i(a_1 + ia_2) & \text{when } \mu = 4. \end{cases} \tag{27}$$

In the above relations, a_1 and a_2 are undetermined magnitudes of the wave field $\hat{u}_{2(i)}$ and the term K^* denotes a wave number normalized with respect to the distance d between two neighboring masses and can be obtained from

$$1 - \frac{\mu(\Omega)}{2} = \begin{cases} \cos\mathsf{K}^* & \text{for } 0 \leq \mu(\Omega) \leq 4 \\ \cosh\mathsf{K}^* & \text{for } \mu(\Omega) < 0 \\ -\cosh\mathsf{K}^* & \text{for } \mu(\Omega) > 4 \end{cases}. \tag{28}$$

The dynamic behavior of the system under consideration can thus be characterized by intervals of frequencies where waves are attenuated in space, i.e. by band gaps. This behavior can be predicted by looking at the effective mass $\mu(\Omega)$: when this function is either negative or larger than 4, a band gap is present.

Fig. 3 represents the graph of $\mu(\Omega)$, given by relations (21) for the two cases under consideration, obtained using the following values for the normalized spring stiffness and the mass ratio

$$\hat{\mathsf{k}} = 4.74, \quad \Theta = 1.18. \tag{29}$$

In the plot, red bands denote band gaps where the effective mass density μ is larger than 4, while blue bands indicate those corresponding to a negative effective mass.

3.2. On the continuous and discrete spectra

What we found in the previous subsection is the continuous spectrum of the discrete Laplacian operator defined on the (discrete) Lebesgue space $\ell^2(\mathbb{Z})$. This problem possesses a real continuous spectrum $\sigma_{\text{c}} = [0, 4]$, that coincides with its essential spectrum σ_{ess} (see e.g. Borthwick, 2020). Therefore, from our results, the effective mass density can be interpreted as the spectrum σ_{ess} of the problem. Indeed, we find that, when μ is such that $0 \leq \mu \leq 4$, then solutions belonging to the space $\ell^2(\mathbb{Z})$ exist and can be represented as superposition of propagating waves (c.f. solution (25)). Outside this range, solutions are no more in that space.

These considerations are only valid when the domain $\mathcal{C}$ of the curvilinear abscissa S is such that $\mathcal{C} = (-\infty, +\infty)$, therefore when we consider a wave propagation problem in an infinite medium. When the domain is bounded by limiting to n the number of elements composing the system, boundary conditions must be taken into account. The problem thus becomes an eigenvalue problem in the space $\ell^2(\mathbb{I})$, with $\mathbb{I} \subset \mathbb{Z}$ being the index set of $\mathcal{P} \subset \mathcal{C}$, that contains the curvilinear abscissas of the elements composing the domain. For the current case the set $\mathcal{P}$ is always non-empty and of finite cardinality $n+2$.

Let us show here how the eigenvalues associated to problem (19) written for solutions in $\ell^2(\mathbb{I})$ are distributed in the spectrum. For this, we fix the boundary conditions to be $\hat{u}_{2(0)} = 0$ and $\hat{u}_{2(n)} = 0$. We then use solution (25), that is valid when $0 \leq \mu \leq 4$. By imposing the boundary condition at $i = 0$, we find

$$a_1 = -a_2. \tag{30}$$

While the boundary condition at $i = n$ gives

$$\sin\mathsf{K}^*(n+1) = 0. \tag{31}$$

From this latter relation, we finally have

$$\mathsf{K}^* = \frac{q\pi}{n+1}, \quad q \in \mathbb{N}, \tag{32}$$

but since $\mathsf{K}^* \in [0, \pi]$, then we find the (preliminary) result that, in each interval where $0 \leq \mu \leq 4$, a maximum number of $n+2$ solutions μ^* can be found using relation (28). This result is an intermediate step.

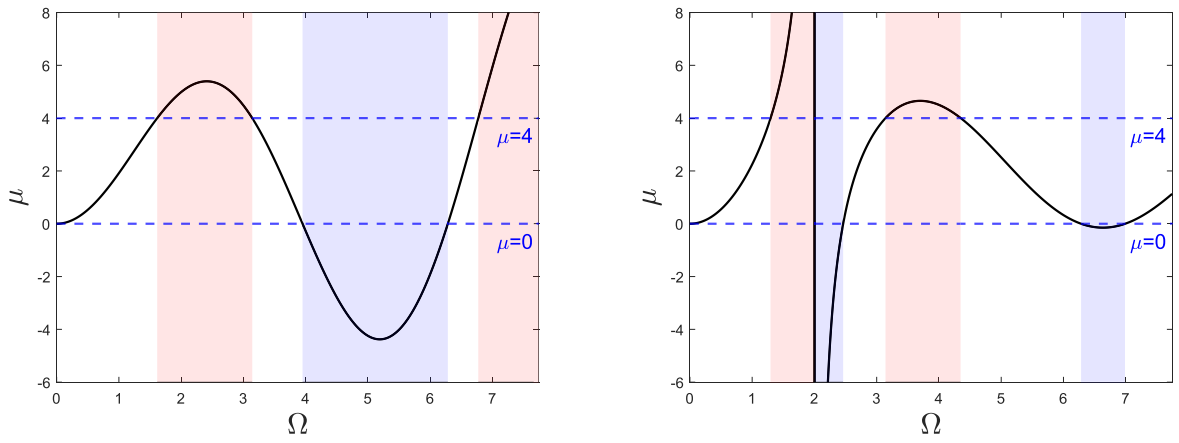

Fig. 3. Graph of the effective mass $\mu(\Omega)$ defined by relation (21), for a cable with (a) masses directly attached on it and (b) masses hanging on it through elastic springs. Shaded areas denote band gaps. (Color figure online.)

3.3. Derivation of the discrete spectrum

Let us now complete the considerations made in Section 3.2. Specifically, we found the intermediate result that $n+2$ potential eigenvalues μ^* can be determined by using relations (28) and (32).

The correct number of eigenvalues μ^* is fixed by considering what happens in each interval $0 \le \mu \le 4$ when $\mathsf{K}^* = 0$ and $\mathsf{K}^* = \pi$, i.e. respectively when $\mu = 0$ and $\mu = 4$. The dimensionless frequencies Ω corresponding to these two cases are found using the definition of the effective mass (21), together with relations (28) and (32). Let us refer to these frequencies as $\hat{\Omega}$. Using condition (30) and relation (25), when either $\mathsf{K}^* = 0$ or $\mathsf{K}^* = \pi$ all the points $\hat{S}_i$ corresponding to the extremities of each interval $((i-1)/(n+1), i/(n+1))$ do not move. Accordingly, to be eigenfrequencies of the whole system, the frequencies $\hat{\Omega}$ must be equal to the (dimensionless) eigenfrequencies of a taut string with a length equal to one interval d, in tension between two fixed supports. Therefore, frequencies $\hat{\Omega}$ corresponding to $\mu = 0$ and to $\mu = 4$ are eigenfrequencies only when they are equal to $j\pi$, with $j \in \mathbb{N}$.[1] We find that, in each pass band, this can happen only for one between $\mu^* = 0$ and $\mu^* = 4$ (this can be demonstrated by studying the behavior of μ using its definition (21) for $\mu = 0$ and $\mu = 4$).

We have thus obtained the following result: *in each interval where* $0 \le \mu \le 4$, *a maximum number of* $n+1$ *eigenvalues* μ^* *can be found.*

In Fig. 4 we show the above result by comparing the continuous and discrete spectra of a cable with 5 attached masses. The continuous spectrum is given by the y-coordinates between 0 and 4. The black curve represents the effective mass density μ, for the two cases shown in Fig. 3. From the previous results, the values of (dimensionless) frequencies of propagating waves are identified by the condition $0 \le \mu \le 4$. The continuous spectrum of the discrete Laplacian operator is thus associated to a family of pass bands for the system. The discrete spectrum is instead obtained by solving the eigenvalue problem in a bounded domain. Considering $n = 5$ masses, using relation (32), six values of K^* are found and the first of relations (28) can be used to determine the corresponding values of μ^*, represented in the figure with the horizontal red dotted lines. The allowed eigenfrequencies, i.e. those corresponding to a solution of the problem, are identified with asterisks as the x-coordinates of the points where the eigenvalues (red dotted lines) intersect the function μ (black curve).

Note that all the eigenfrequencies are grouped within the pass bands of the problem in the unbounded domain. This can also be explained by looking at the solutions (26) valid for frequencies within a band gap: corresponding to superpositions of exponentials, these solutions cannot fulfill the boundary conditions of the problem.

3.4. Mode localization with a defect of periodicity

Let us now deal with the localization problem. As specified in the introductory section, this phenomenon can be studied for the structural model analyzed by introducing a compact perturbation of its periodic composition. This defect might represent a local imperfections to the assumed perfect periodicity. We here limit ourselves to the case when the masses can be considered as directly attached to the cable, as this will be the system later used for the experimental tests.[2] More specifically, we aim to analyze the system reported in Fig. 5, where the cable is shown in its horizontal static equilibrium configuration with a family of masses represented again by filled black dots. An empty circle indicates a mass that has been removed from the system. Accordingly, we are dealing with a domain presenting a periodic array of scatter elements, where a defect is generated by removing the scatterer from the central unit cell.

As the discrete Laplacian operator on $\ell^2(\mathbb{Z})$ is self-adjoint, it conserves its essential spectrum when locally perturbed (from a corollary of Weyl's theorem, see e.g. Reed and Simon, 1978). It follows that, if an eigenvalue exists in the spectrum of the perturbed operator, it will be of finite multiplicity and its corresponding eigenmode will decay exponentially outside the defect, where it will be localized.

This localization phenomenon remains valid also when the domain is bounded. From a physical point of view, the system can be decomposed in three regions as in Fig. 5, with two barriers composed of a periodic domain and one defective region where a mass element is removed. We thus have two possible situations:

i. within the two barriers, solutions of the form (25) can still exist and can be matched with a standing wave within the defect. From the results of the previous subsection, eigenmodes of this form must belong to a pass band in the continuous spectrum of the unperturbed operator;
ii. within the two barriers, solutions of the form (26) can exist as well. A standing wave in the defect could be generated at a frequency within a band gap for the unperturbed operator

[1] We here consider $j = 0$, although the corresponding eigenfrequency is not part of the spectrum. Since we are looking for solutions to the problem, we also take into account this case corresponding to $\hat{u}_2(\hat{S}) = 0$ everywhere.

[2] Note that the very same behavior can also affect the cable with hanging masses.

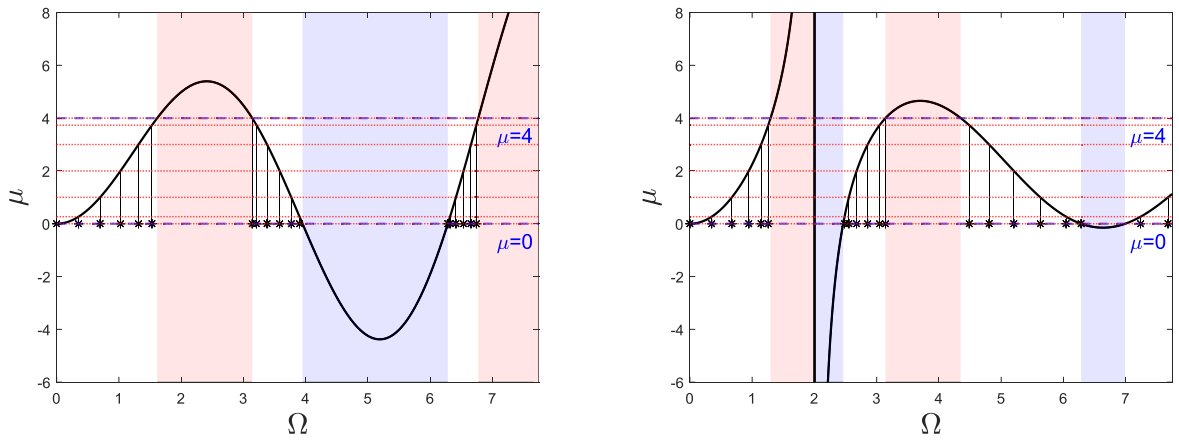

Fig. 4. The intersections of the eigenvalues μ^* (red dotted lines) with the graph of μ (black curve) give the eigenfrequencies of the problem (asterisks along the x-axis), for $n = 5$ masses along a cable when (a) they are directly attached and when (b) they are hanging. (For interpretation of the references to color in this figure legend, the reader is referred to the web version of this article.)

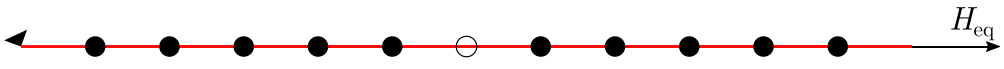

Fig. 5. Taut string with a periodic arrangement of attached masses, represented as black dots. The empty circle denotes a removed mass.

and matches the solutions in the barriers, that can exponentially decay towards the two ends of the domain to fulfill the boundary conditions. In particular, by placing the position $i = 0$ at the point where the mass is missing inside the defect and by using relations (26), applying the continuity of the displacement at $i = 0$ we obtain:

$$\hat{u}_{2(i)} = \begin{cases} A \exp\{-\mathsf{K}^* |i|\} & \text{for } \mu(\Omega) < 0 \\ A(-1)^i \exp\{-\mathsf{K}^* |i|\} & \text{for } \mu(\Omega) > 4 \end{cases} \quad \forall i \in \mathcal{P}, \tag{33}$$

where A is a constant of integration.

These results are shown in Fig. 6. Specifically, as we described before, the essential spectrum of the discrete Laplacian operator here considered ($0 \leq \mu \leq 4$) corresponds to pass bands for the system, represented to the white bands in Fig. 6. These regions identify the essential spectrum in terms of frequencies and they are conserved when dealing with the perturbed operator. The red dotted vertical lines in the figure identify the eigenvalues (indicated with an asterisk) of the bounded problem with a defect. One can check from the figure that, although the majority of the eigenvalues are still grouped inside pass bands for the unbounded problem (situation (i) above), some of them are inside a band gap (situation (ii) above). This behavior is different with respect to the case studied in Fig. 4, where no defect was present in the system. In particular, the eigenmodes inside a band gap correspond to a motion of the cable that is localized within the defect, as can be seen in Fig. 6(b) where we plot the modal shapes of the first localized eigenmode for the analyzed cases.

When the number of masses is increased, for example considering a cable with $n = 11(-1)$, the eigenvalues fill more and more the pass bands (cf. Fig. 6(c)) and the defect causes an eigenmode in the first band gap characterized by a stronger localization of the motion in the cavity (cf. Fig. 6(d)).

4. Experimental validation

In this section we aim to verify the theoretical results previously described by means of an experimental test. We consider here the case of a cable with a family of masses that are directly attached on it.

4.1. Setup of the test

The experimental setup is shown in Fig. 7(a). The mechanical system is made up of a taut steel string with an array of lead spheres of mass M, i.e. of scatter elements, periodically inserted on the cable and glued to it by means of beeswax. The cable is in tension between two supports. In particular, the left end is fixed to a *load cell* for measuring the tension H_{eq} initially applied to the cable. The right boundary is instead fixed along the horizontal direction and supported by the head of a *K2007E01 shaker* in the vertical direction. The system is characterized by the parameters given in Table 1. The total weight of the system with 11 lead masses is $W = 0.057$ N, while the static initial tension is $H_{\text{eq}} = 10$ N $\gg W$, hence the static equilibrium configuration can be considered horizontal (zero initial sag). Consequently, the same is valid also for the system with 5 masses. The shaker is used to trigger the free oscillations of the cable in the vertical plane around this equilibrium configuration. The shaker is carefully adjusted so that the initial displacement is only vertical. This point is critical to avoid parametric excitation that would modify the motion of the cable (Nayfeh et al., 1995). The voltage signal that is then converted into motion of the shaker head at the support is given by an *Agilent 33 500 series 30 MHz function/arbitrary wave form generator*.

Due to the lightness of the system, we used a contact-less measurement device to study the motion of the cable. To this end, we have employed several *CNY70 reflective optical sensors with transistor output*. These instruments include an infrared emitter and a photo-transistor in a leaded package which blocks visible light. When the target moves, the voltage output from the optical sensor can be recorded and, after the calibration of the sensor, one can read a variation of the position of the target object. Therefore, placing these optical devices below the cable, we are able to read the vertical displacement of the cable points above these sensors and to study the cable response to the imposed motion at the right support. To enhance the reflection, small pieces of white tape are glued at the cable points above the sensors, constituting the target objects for the measures taken by each sensor (cf. Fig. 7(b)).

A total of 5 sensors of this type are employed along the system. To measure the actual imposed motion at the right support, we employ one more sensor (labeled sensor 0) above the head of the shaker (cf. Fig. 7(c)).

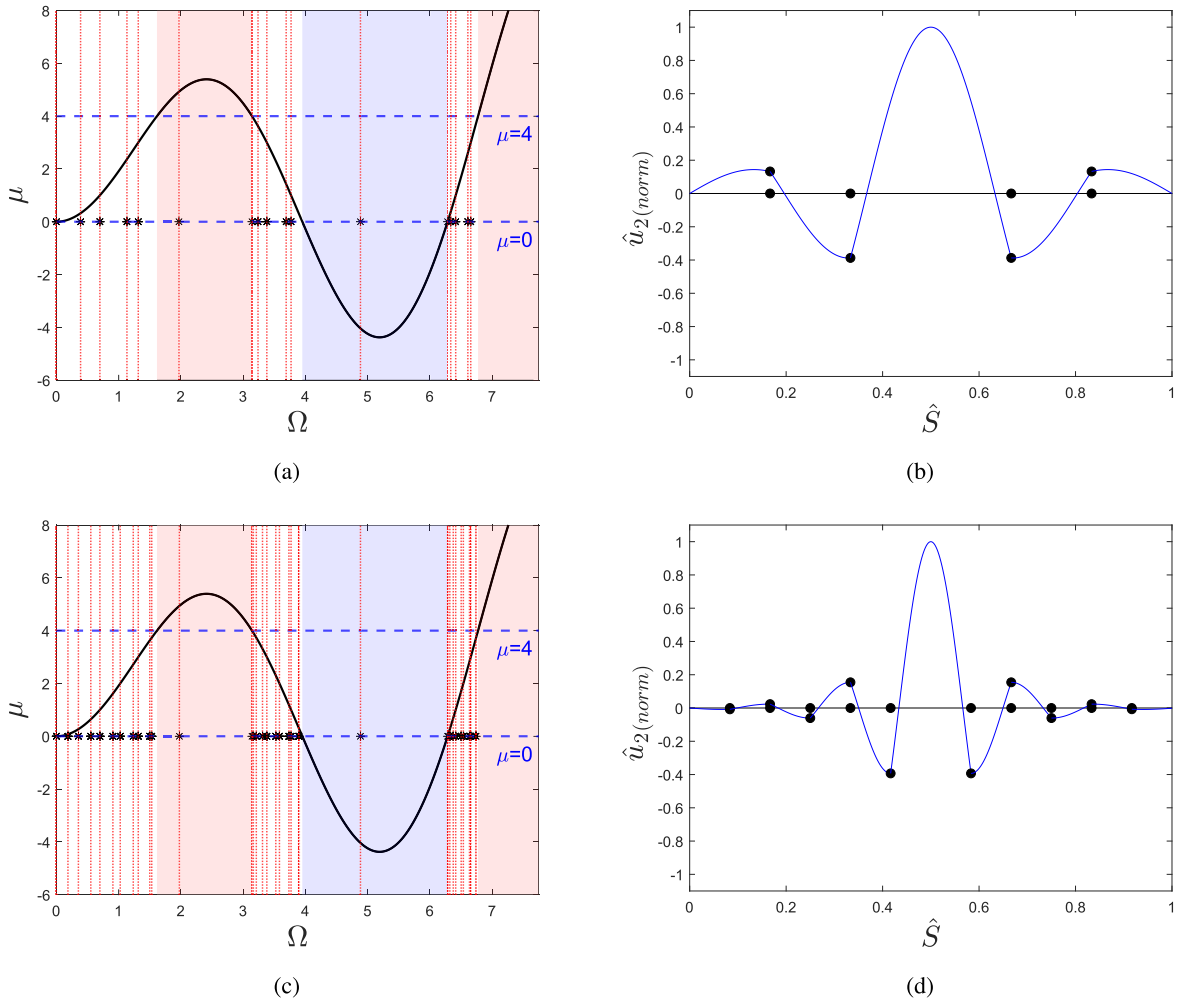

Fig. 6. In (a) and (c), spectra of a cable with respectively $n = 5\,(-1)$ and $n = 11\,(-1)$ masses (from a system of n masses, one is removed) directly attached to the cable. Black curves represent the effective mass density μ. Red dashed vertical lines, in correspondence of the asterisk along the x-axis, give the (dimensionless) eigenfrequencies when the cable has a central defect (central mass removed). In (b) and (d), modal shapes of the eigenvalues inside the first band gap respectively of subfigures (a) and (c). The black dots indicate the position of the masses. (For interpretation of the references to color in this figure legend, the reader is referred to the web version of this article.)

We point out that these optical devices allow for a low-budget test, that, considering the smallness of the target (i.e. the cable section) and the frequencies under study, makes this method a very attractive solution.

4.2. Results and discussion

We consider both the case when n masses are periodically arranged along the cable and the case when a defect of periodicity is introduced by removing the central mass from the system.

4.2.1. Periodic system

Our aim is to locate the natural frequencies, corresponding to a primary resonance condition for the cable under study, and to compare them with those obtained from the prior theoretical considerations. We trigger the free vibrations of the system by a small vertical displacement (namely the maximum amplitude imposed by the shaker is lower than 0.07% of the cable length) to keep the generated vertical motion along the cable small enough to avoid as much as possible the activation of non-linear phenomena.

To identify the eigenvalues experimentally, we excite the cable with a Gaussian-modulated sinusoidal wave directly created using the wave form generator. Fig. 8(a) shows the time variation in volts of the Gaussian-modulated sinusoidal signal created using the wave form generator.

Table 1
Material and geometrical parameters used for the experimental test.

ρ_R [kg/m]	E [Pa]	A_R [m^2]	ℓ_R [m]	n	H_{eq} [N]	M [kg]
1.52×10^{-3}	2.3×10^{11}	1.96×10^{-7}	1.21	5	≈10	3.6×10^{-4}

The corresponding frequency content is computed with the Matlab FFT algorithm and is given in Fig. 8(b) in terms of *Power Spectrum* (PS) normalized with respect to its maximum value and expressed in decibels (dB).

In Fig. 8(a), we also report the actual displacement imposed to the cable (red curve), as measured by sensor 0. Note that there is a difference between the signal and the generated displacement. This is mainly due to the fact that the shaker is influenced by the response of the cable and is not able to perfectly reproduce the generated signal.

To study the attenuation properties of the ideal unbounded periodic system, one should input a wave and measure the spatial decay along the system, which is expected for frequencies inside a band gap. However, as the experimental setup has boundaries, we must use the results obtained for a finite system. In particular, we have previously shown that, although with boundaries the concept of continuous spectrum and thus of band gaps is lost, its effect is still valid in the sense that the eigenfrequencies of the problem are only grouped in the pass bands of the unbounded domain. This is true when no defects are present. If

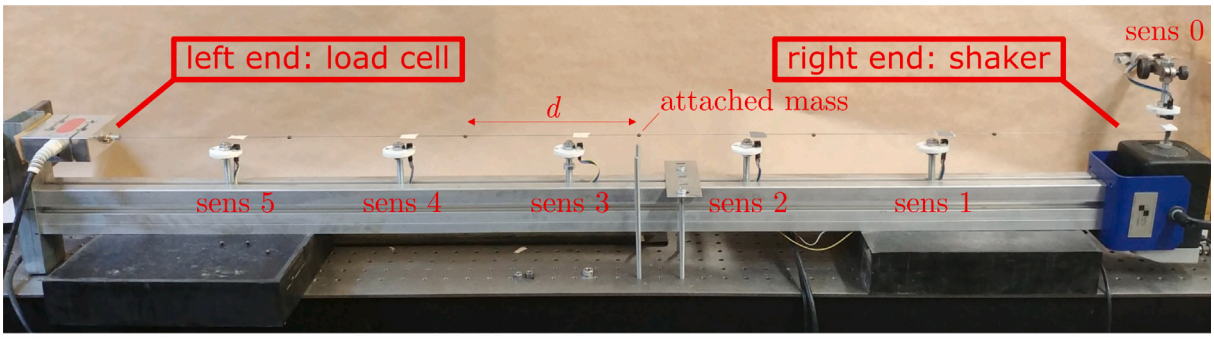

(a)

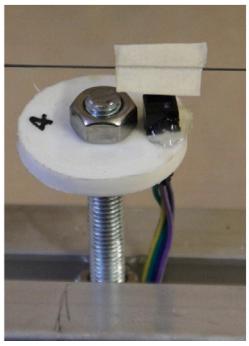

(b)

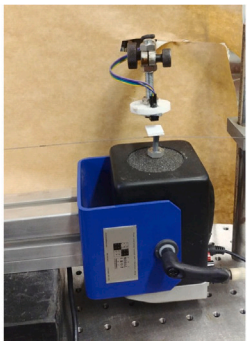

(c)

Fig. 7. Experimental setup (a). The whole system composed of the cable with attached masses, in tension between a load cell at the left boundary and a shaker at the right boundary, that imposes a vertical motion. Five optical sensors are distributed below the cable. The cable points above these sensors are equipped with a square white piece of tape to enable the measurement of the vertical displacement of the cable with the optical sensors. Zoom over (b) the sensor number 4 used in the system and over (c) the shaker at the right boundary.

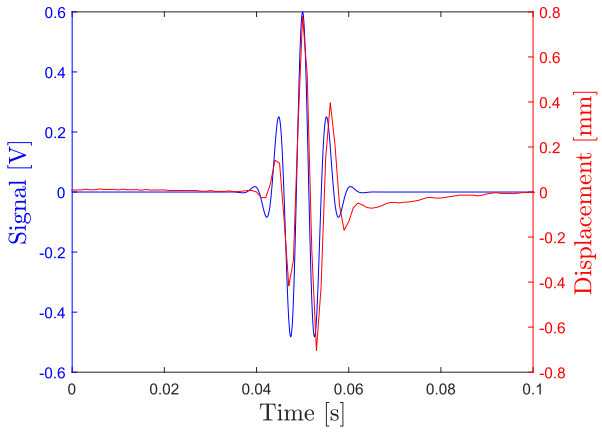

(a)

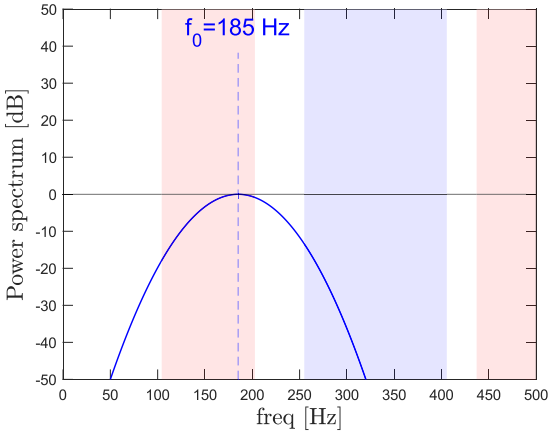

(b)

Fig. 8. (a) Time series of the Gaussian-modulated sinusoidal signal used as input for the waveform generator (in blue) and the corresponding imposed displacement (in red). "V" stands for Volts. (b) Frequency content of the input signal. Shaded regions denote band gaps for the unbounded problem. (For interpretation of the references to color in this figure legend, the reader is referred to the web version of this article.)

there is a defect, we expect to find some eigenvalues inside a band gap, corresponding to localized eigenmodes.

Let us consider the input signal shown in Fig. 8. The response will thus be composed of a short transitory phase needed for the activation of the eigenmodes of the bounded problem, followed by a free motion phase during which the input pulse is already ended and the excited eigenmodes decay, at different rates, due to damping. We report in Fig. 9 the Fourier transforms of the signals measured by the 5 sensors along the cable for the imposed motion given in Fig. 8(a), when no masses are removed (case without a defect). The results are given in terms of Transmission (T), defined as

$$T := 10\ \mathrm{Log}\left(\frac{\left|PS_j\right|}{\max\limits_{\mathrm{freq}}\left|PS_0\right|}\right)^2, \tag{34}$$

where PS_j, with j from 0 to 5, denotes the Power Spectrum of the signal measured by the jth sensor.

The Frequency Response Function of the Gaussian-modulated imposed displacement ($j = 0$ in relation (34)) is also reported in Fig. 9

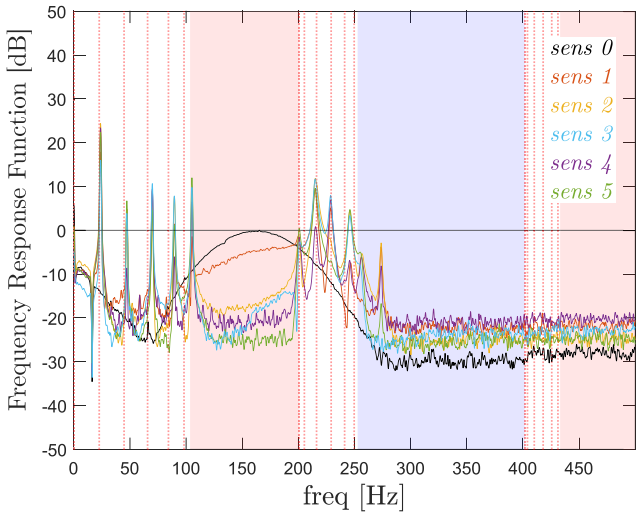

Fig. 9. Results from a Gaussian-modulated sinusoidal excitation: Power Spectrum (PS) of the signals from sensor 1 to 5, normalized with respect to the maximum value of the PS from sensor 0, reported with a black curve in the plot. (For interpretation of the references to color in this figure legend, the reader is referred to the web version of this article.)

(black curve). The banded structure of the spectrum is clear. In particular, one can see that the modes within the first two pass bands are activated. Conversely, no modes are visible from the third pass band, as it is expected by looking at the curve of the input signal: its frequency content is negligible above approximately 300 Hz.

Contrary to what happens for the lower modes in the first pass band, the agreement between the PS peaks and the theoretical eigenfrequencies (indicated by the vertical dashed red lines) is not very good for the higher modes of the second pass band. In particular the experimentally obtained eigenfrequencies are slightly moved at higher frequencies with respect to the theoretical ones. This can be due to the presence of the tape used as target object for the measurements of the cable motion, that influences the dynamics of the cable. The system is indeed more affected by experimental imperfections at higher frequencies.

We can also reconstruct the motion of the system from the cable points positioned above the 5 optical sensors. In particular, at an eigenfrequency of the bounded problem, the system should move according to the corresponding modal shape.

As an example, Fig. 10 shows the comparison between the third mode analytically computed (a) and the experimental one, reconstructed through the sensors measurements (b). Black dots stand for masses, whereas black circles denote the material points above the sensors. The results are in good agreement for the mode under consideration.

From the test, we can also check the behavior of the system for frequencies belonging to a band gap. In Fig. 11, we report the motion of the tested cable at the frequencies $f = 165$ Hz (left) and $f = 185$ Hz (right). Specifically, we find that the wave in the system is characterized by an amplitude that is attenuated from the moving support (right end) to the fixed support (left end), verifying the presence of a band gap in the spectrum. Moreover, at $f = 165$ Hz (Fig. 11(a)) the attenuation is stronger then at $f = 185$ (Fig. 11(b)). This latter frequency is indeed positioned closer to the edge of the first band gap and, accordingly, one expects less attenuation.

4.2.2. System with a defect

The system then was tested by removing the central mass from the first configuration of 5 masses. For this, we use again the Gaussian-modulated sinusoidal input signal depicted in Fig. 8, centered at a frequency of 185 Hz. The content in frequency of this signal is sufficiently high both inside the first band gap and the second pass band. Accordingly, from our previous theoretical results, we expect to activate both the defect mode at the frequency $f \approx 127$ Hz, corresponding to the localized modal shape reported in Fig. 6(c), and the eigenfrequencies belonging to the second pass band. This is indeed verified as shown in Fig. 12, where we report the Fourier transform of the signals acquired by the optical sensors. Note also that from sensor 1 to 5 the content at the frequencies belonging to the first band gap is decreasing, except at the frequency where a localized mode is expected. This confirms the attenuating behavior due to the presence of the scatter elements and the localization capabilities of the system caused by the removal of one mass from the periodic arrangement.

The modal shape of the defect mode is compared in Fig. 13 (first row) with the behavior of the tested cable at the corresponding frequency. A good agreement between the two results is obtained, with the motion being maximum within the defect.

Eventually, we report in Fig. 13 (second row) the response of the cable when the number of masses in the perfectly periodic system is increased to 11 and the central mass is removed. Note that, for this case, the force imposed to the system was reduced to $H_{\text{eq}} = 3.4$ N to lower the frequencies of the second pass band. From the theoretical results, a peak is expected inside the first band gap at a frequency $f \approx 134$ Hz. The corresponding modal shape, reported in Fig. 6(d) and represented again here in Fig. 13(c), agrees with the response obtained from the experiment, reported in Fig. 13(d), even though more optical sensors should be used along the cable to better reconstruct the rapid spatial variation. As we specified before in Section 3.4, as the number of masses is larger, the motion is more concentrated in the defect.

5. Concluding remarks

In this work, 1D cable systems with periodic arrangements of suspended masses were investigated. We here gave a preliminary proof that their dynamics can be characterized by an attenuating behavior in specific frequency ranges. For this, small oscillations of a taut string with a family of hanging masses were considered. This problem was also studied by other authors (Pakos, 2019; Liu et al., 2022), who mainly focused on effective ways to obtain the modal response of the system. We found that the problem is actually governed by the same equation valid for 1D periodic discrete domains, with the spectrum being thus characterized by band gaps and pass bands, whose position in the frequency domain can be derived from a frequency dependent effective mass, whose behavior is related to the specific system under consideration. This is a condition typically searched when dealing with metamaterials (or metastructures). The present analysis, based on the interpretation as metastructure, allows to obtain analytical predictions of the "structure" of the spectrum, highlighting the influence of the various material and geometric parameters.

We showed that, when dealing with a bounded domain for the cable, the spectrum of the problem becomes discrete. The eigenfrequencies can only be positioned inside a pass band of the continuous spectrum associated to the same problem expressed for the unbounded domain. This is no more true when a defect is introduced, e.g. by removing one mass from the periodic array. A localization phenomenon can take place, with modes entering the band gaps.

The described theoretical results were compared with those obtained from experimental tests. A good agreement between the two was observed.

The results obtained are limited by the linearization of the original problem. An interesting extension of the present work would be that of understanding how the band gaps change when the equilibrium configuration of the cable is no more horizontal. It is known that, in the case of a bare cable suspended between two fixed supports, the eigenfrequencies of the associated problem are strongly affected by the actual static equilibrium configuration (Irvine and Griffin, 1976).

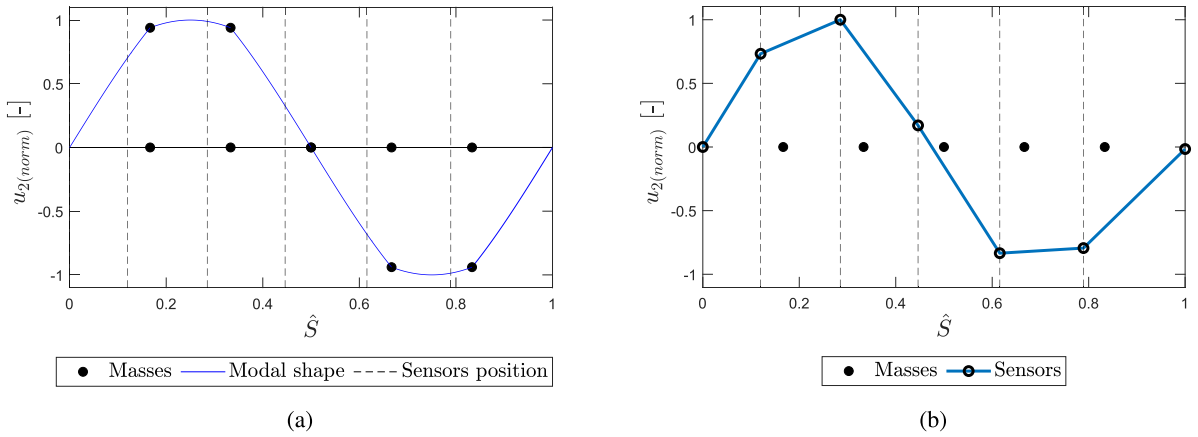

Fig. 10. Comparison between modal shapes (a), and motion of the tested system (b), for the third eigenmode at $f \approx 46$ Hz. Black dots stand for masses, black circles and vertical dashed lines for points above the optical sensors.

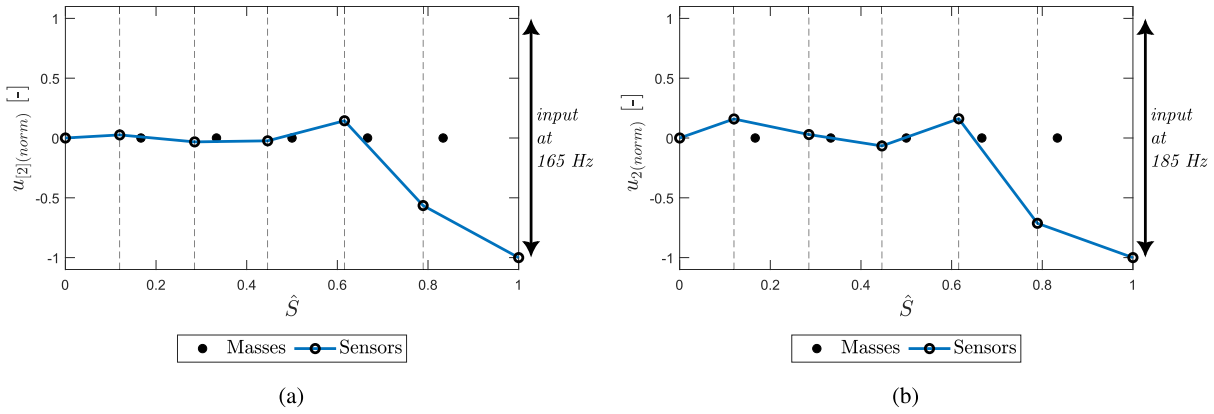

Fig. 11. Motion of the tested cable at (a) $f = 165$ Hz and (b) $f = 185$ Hz. Black dots stand for masses, black circles and vertical dashed lines for points above the optical sensors.

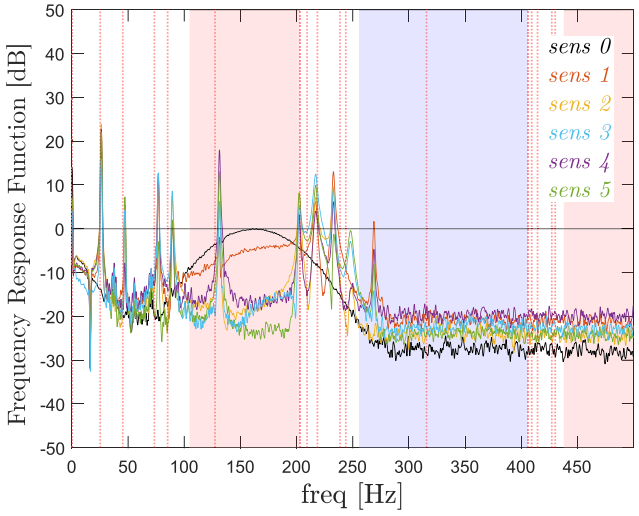

Fig. 12. Results from a Gaussian-modulated sinusoidal excitation for the system with a defect: PS of the signals from sensors 1 to 5, normalized with respect to the maximum value of the PS from sensor 0, reported with a black curve in the plot. Logarithmic scale is used. (For interpretation of the references to color in this figure legend, the reader is referred to the web version of this article.)

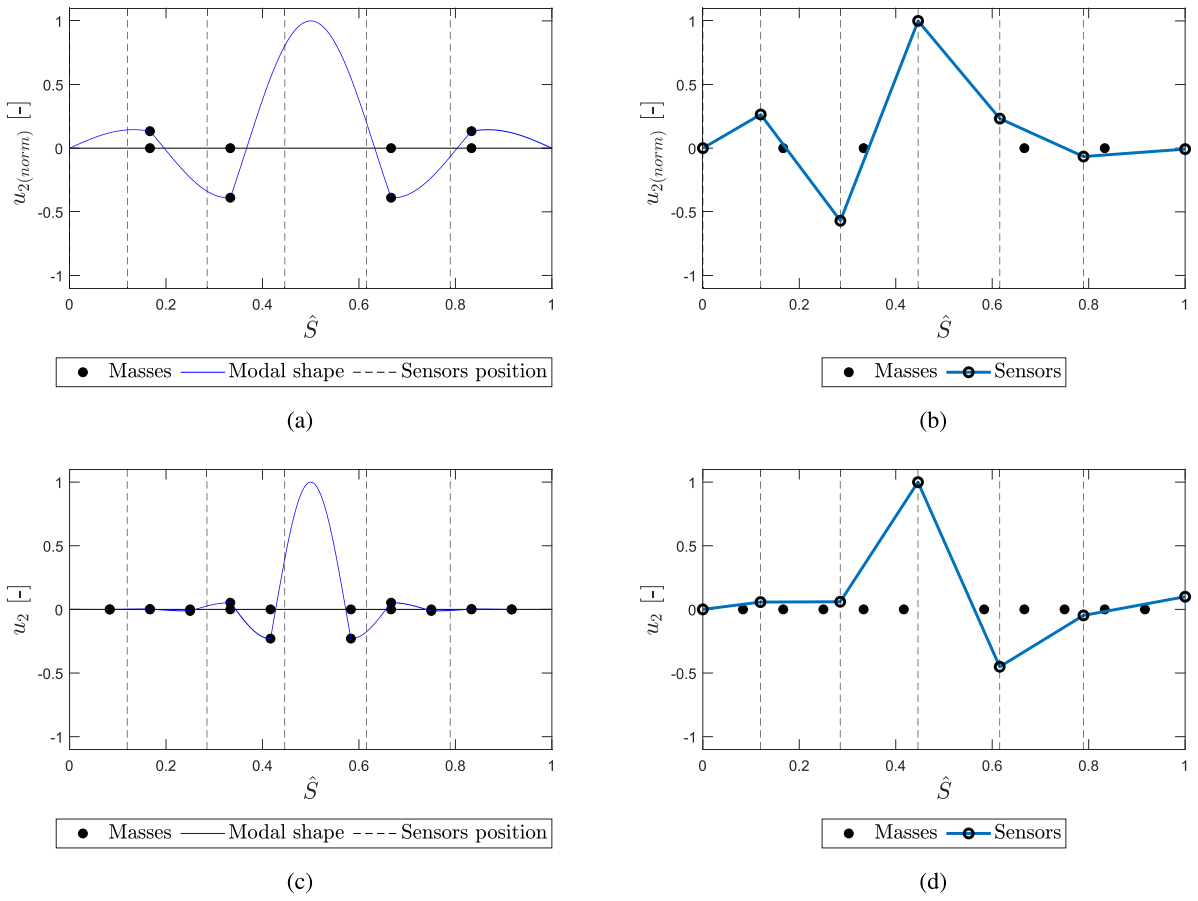

Fig. 13. Comparison between modal shapes and motion of the tested system. (a) and (b) for the system with $5(-1)$ masses and a theoretical peak at $f \approx 127$ Hz. (c) and (d) for the system with $11(-1)$ masses and a theoretical peak at $f \approx 134$ Hz. Black dots stand for masses, black circles and vertical dashed lines for points above the optical sensors.

Concerning the problem of wave propagation associated to cables with a family of scatter elements, we thus expect that the band gaps found for a horizontal initial configuration can be similarly impacted. Furthermore, cables dynamics is very soon affected by geometric nonlinear effects. These phenomena are of course of interest also when dealing with periodic cable systems. The established interpretation of the dynamic behavior of periodic cables with that of periodic metamaterials could be possibly extended to the nonlinear scenario, to build a general framework for the problem.

CRediT authorship contribution statement

Marco Moscatelli: Writing – original draft, Investigation, Conceptualization. **Claudia Comi:** Writing – original draft, Investigation, Conceptualization. **Jean-Jacques Marigo:** Writing – original draft, Investigation, Conceptualization.

Declaration of competing interest

The authors declare that they have no known competing financial interests or personal relationships that could have appeared to influence the work reported in this paper.

Data availability

No data was used for the research described in the article.

Acknowledgments

We acknowledge Marco Cucchi from the "Laboratorio Prove Materiali" (LPM) at Politecnico di Milano for his help in the realization of the experimental tests.

References

Ammari, H., Hiltunen, E.O., Yu, S., 2022. Subwavelength guided modes for acoustic waves in bubbly crystals with a line defect. J. Eur. Math. Soc. 24 (7), 2279–2313. http://dx.doi.org/10.48550/arXiv.1904.04512.

Anderson, P.W., 1958. Absence of diffusion in certain random lattices. Phys. Rev. 109 (5), 1492–1505. http://dx.doi.org/10.1103/PhysRev.109.1492.

Borthwick, D., 2020. Spectral Theory. Springer International Publishing, p. 338. http://dx.doi.org/10.1007/978-3-030-38002-1.

Demeio, L., Lenci, S., 2022. Periodic traveling waves in a taut cable on a bilinear elastic substrate. Appl. Math. Model. 110, 603–617. http://dx.doi.org/10.1016/j.apm.2022.06.009.

Figotin, A., Klein, A., 1994. Localization phenomenon in gaps of the spectrum of random lattice operators. J. Stat. Phys. 75 (5–6), 997–1021. http://dx.doi.org/10.1007/BF02186755.

Figotin, A., Klein, A., 1996. Localization of classical waves I: Acoustic waves. Comm. Math. Phys. 180 (2), 439–482. http://dx.doi.org/10.1007/BF02099721.

Figotin, A., Klein, A., 1997. Localized classical waves created by defects. J. Stat. Phys. 86 (1–2), 165–177. http://dx.doi.org/10.1007/BF02180202.

Fliss, S., Joly, P., 2012. Wave propagation in locally perturbed periodic media (case with absorption): Numerical aspects. J. Comput. Phys. 231 (4), 1244–1271. http://dx.doi.org/10.1016/j.jcp.2011.10.007.

He, C., Lim, K.M., Liang, X., Zhang, F., Jiang, J., 2022. Tunable band structures design for elastic wave transmission in tension metamaterial chain. Eur. J. Mech. A Solids 92, 104481. http://dx.doi.org/10.1016/j.euromechsol.2021.104481.

Irvine, M., 1981. Cable Structures. The Massachusetts Institute of Technology, Cambridge, p. 259.

Irvine, H.M., Griffin, J.H., 1976. On the dynamic response of a suspended cable. Earthq. Eng. Struct. Dyn. 4 (4), 389–402. http://dx.doi.org/10.1002/eqe.4290040406.

Joannopoulos, J.D., Johnson, S.G., Winn, J.N., Meade, R.D., 2008. Photonic Crystals: Molding the Flow of Light (Second Edition). Princeton University Press, p. 446.

Khelif, A., Choujaa, A., Djafari-Rouhani, B., Wilm, M., Ballandras, S., Laude, V., 2003. Trapping and guiding of acoustic waves by defect modes in a full-band-gap ultrasonic crystal. Phys. Rev. B 68 (21), 214301. http://dx.doi.org/10.1103/PhysRevB.68.214301.

Krushynska, A.O., Anerao, N., Badillo-Ávila, M.A., Stokroos, M., Acuautla, M., 2021. Arbitrary-curved waveguiding and broadband attenuation in additively manufactured lattice phononic media. Mater. Des. 205, 109714. http://dx.doi.org/10.1016/j.matdes.2021.109714.

Laude, V., 2015. Phononic Crystals. DE GRUYTER, Berlin, München, Boston.

Laude, V., 2021. Principles and properties of phononic crystal waveguides. APL Mater. 9 (8), 080701. http://dx.doi.org/10.1063/5.0059035.

Liu, D., Jia, C., Song, B., Li, D., 2022. Singular function model of concentrated mass-cable composite structures. J. Vib. Eng. Technol. 10 (7), 2657–2667. http://dx.doi.org/10.1007/s42417-022-00510-2.

Maurel, A., Marigo, J.-J., Mercier, J.F., Pham, K., 2018. Modelling resonant arrays of the Helmholtz type in the time domain. Proc. R. Soc. A Math. Phys. Eng. Sci. 474 (2210), http://dx.doi.org/10.1098/rspa.2017.0894.

Milton, G.W., Briane, M., Willis, J.R., 2006. On cloaking for elasticity and physical equations with a transformation invariant form. New J. Phys. 8 (10), 248. http://dx.doi.org/10.1088/1367-2630/8/10/248.

Miniaci, M., Krushynska, A., Bosia, F., Pugno, N.M., 2016. Large scale mechanical metamaterials as seismic shields. New J. Phys. 18 (8), 083041. http://dx.doi.org/10.1088/1367-2630/18/8/083041.

Moscatelli, M., 2022. Metamaterials for energy harvesting at small scale (Ph.D. thesis). École polytechnique, Palaiseau (France), p. 187, URL: https://theses.hal.science/tel-03714470.

Moscatelli, M., Comi, C., Marigo, J.-J., 2021. On the dynamic behaviour of discrete metamaterials: From attenuation to energy localization. Wave Motion 104, 102733. http://dx.doi.org/10.1016/j.wavemoti.2021.102733.

Nayfeh, A.H., Frank Pai, P., 2008. Linear and Nonlinear Structural Mechanics. Wiley, p. 763.

Nayfeh, A.H., Mook, D.T., 1995. Nonlinear Oscillations. Wiley, p. 720.

Nayfeh, S.A., Nayfeh, A.H., Mook, D.T., 1995. Nonlinear response of a taut string to longitudinal and transverse end excitation. J. Vib. Control 1 (3), 307–334. http://dx.doi.org/10.1177/107754639500100304.

Pakos, W., 2019. Free vibration of a sagged cable with attached discrete elements. Appl. Math. Mech. 40 (5), 631–648. http://dx.doi.org/10.1007/s10483-019-2479-6.

Palermo, A., Krödel, S., Marzani, A., Daraio, C., 2016. Engineered metabarrier as shield from seismic surface waves. Sci. Rep. 6 (1), 1–10. http://dx.doi.org/10.1038/srep39356.

Pendry, J.B., 2000. Negative refraction makes a perfect lens. Phys. Rev. Lett. 85 (18), 3966–3969. http://dx.doi.org/10.1103/PhysRevLett.85.3966.

Reed, M., Simon, B., 1978. Methods of Modern Mathematical Physics. IV, Analysis of Operators. Academic Press, New York, NY, p. 325.

Rega, G., 2004a. Nonlinear vibrations of suspended cables—Part I: Modeling and analysis. Appl. Mech. Rev. 57 (6), 443–478. http://dx.doi.org/10.1115/1.1777224.

Rega, G., 2004b. Nonlinear vibrations of suspended cables—Part II: Deterministic phenomena. Appl. Mech. Rev. 57 (6), 479–514. http://dx.doi.org/10.1115/1.1777225.

Rosafalco, L., De Ponti, J.M., Iorio, L., Ardito, R., Corigliano, A., 2023. Optimised graded metamaterials for mechanical energy confinement and amplification via reinforcement learning. Eur. J. Mech. A Solids 99, 104947. http://dx.doi.org/10.1016/j.euromechsol.2023.104947.

Santosa, F., Ammari, H., 2004. Guided waves in a photonic bandgap structure with a line defect. SIAM J. Appl. Math. 64 (6), 2018–2033. http://dx.doi.org/10.1137/S0036139902404025.

Schurig, D., Mock, J.J., Justice, B.J., Cummer, S.A., Pendry, J.B., Starr, A.F., Smith, D.R., 2006. Metamaterial electromagnetic cloak at microwave frequencies. Sci. (80-.). 314 (5801), 977–980. http://dx.doi.org/10.1126/science.113328.

Sigalas, M.M., 1997. Elastic wave band gaps and defect states in two-dimensional composites. J. Acoust. Soc. Am. 101 (3), 1256–1261. http://dx.doi.org/10.1121/1.418156.

Sigalas, M.M., 1998. Defect states of acoustic waves in a two-dimensional lattice of solid cylinders. J. Appl. Phys. 84 (6), 3026–3030. http://dx.doi.org/10.1063/1.368456.

Torrent, D., Sánchez-Dehesa, J., 2008. Acoustic cloaking in two dimensions: A feasible approach. New J. Phys. 10 (6), 063015. http://dx.doi.org/10.1088/1367-2630/10/6/063015.

Wilcox, S., Botten, L.C., McPhedran, R.C., Poulton, C.G., De Sterke, C.M., 2005. Modeling of defect modes in photonic crystals using the fictitious source superposition method. Phys. Rev. E - Stat. Nonlinear, Soft Matter Phys. 71 (5), http://dx.doi.org/10.1103/PhysRevE.71.056606.

Yang, X., Yin, J., Yu, G., Peng, L., Wang, N., 2015. Acoustic superlens using Helmholtz-resonator-based metamaterials. Appl. Phys. Lett. 107 (19), 193505. http://dx.doi.org/10.1063/1.4935589.